

Bessel-Gaussian beam-based orbital angular momentum holography

Jiaying Ji(季佳滢), Zhigang Zheng(郑志刚), Jialong Zhu(朱家龙), Le Wang(王乐), Xinguang Wang(王新光), and Shengmei Zhao(赵生妹)

Citation: Chin. Phys. B, 2024, 33 (**1**): 014204. DOI: 10.1088/1674-1056/acfdff

Journal homepage: http://cpb.iphy.ac.cn; http://iopscience.iop.org/cpb

What follows is a list of articles you may be interested in

Spin splitting of vortex beams on the surface of natural biaxial hyperbolic materials

Hong Liang(梁红), Haoyuan Song(宋浩元), Yubo Li(李宇博), Di Yu(于迪), and Shufang Fu(付淑芳)

Chin. Phys. B, 2023, 32 (**12**): 124212. DOI: 10.1088/1674-1056/ad0ccc

Diffraction deep neural network based orbital angular momentum mode recognition scheme in oceanic turbulence

Hai-Chao Zhan(詹海潮), Bing Chen(陈兵), Yi-Xiang Peng(彭怡翔), Le Wang(王乐), Wen-Nai Wang(王文鼐), and Sheng-Mei Zhao(赵生妹)

Chin. Phys. B, 2023, 32 (**4**): 044208. DOI: 10.1088/1674-1056/ac935e

Atomic optical spatial mode extractor for vector beams based on polarization-dependent absorption

Hong Chang(常虹), Xin Yang(杨欣), Jinwen Wang(王金文), Yan Ma(马燕), Xinqi Yang(杨鑫琪), Mingtao Cao(曹明涛), Xiaofei Zhang(张晓斐), Hong Gao(高宏), Ruifang Dong(董瑞芳), and Shougang Zhang(张首刚)

Chin. Phys. B, 2023, 32 (**3**): 034207. DOI: 10.1088/1674-1056/acac19

Generation of elliptical airy vortex beams based on all-dielectric metasurface

Xiao-Ju Xue(薛晓菊), Bi-Jun Xu(徐弼军), Bai-Rui Wu(吴白瑞), Xiao-Gang Wang(汪小刚), Xin-Ning Yu(俞昕宁), Lu Lin(林露), and Hong-Qiang Li(李宏强)

Chin. Phys. B, 2023, 32 (**2**): 024215. DOI: 10.1088/1674-1056/ac7cd0

Asymmetrical spiral spectra and orbital angular momentum density of non-uniformly polarized vortex beams in uniaxial crystals

Ling-Yun Shu(舒凌云), Ke Cheng(程科), Sai Liao(廖赛), Meng-Ting Liang(梁梦婷), and Ceng-Hao Yang(杨嶒浩)

Chin. Phys. B, 2023, 32 (**2**): 024211. DOI: 10.1088/1674-1056/ac7860

Bessel–Gaussian beam-based orbital angular momentum holography

Jiaying Ji(季佳滢)[1], Zhigang Zheng(郑志刚)[1], Jialong Zhu(朱家龙)[1], Le Wang(王乐)[1], Xinguang Wang(王新光)[1], and Shengmei Zhao(赵生妹)[1,2,3,†]

[1] *Institute of Signal Processing and Transmission, Nanjing University of Posts and Telecommunications (NJUPT), Nanjing* 210003, *China*
[2] *Key Laboratory of Broadband Wireless Communication and Sensor Network Technology, Ministry of Education, Nanjing* 210003, *China*
[3] *National Laboratory of Solid State Microstructures, Nanjing University, Nanjing* 210093, *China*

(Received 19 July 2023; revised manuscript received 3 September 2023; accepted manuscript online 28 September 2023)

Orbital angular momentum (OAM), as a new degree of freedom, has recently been applied in holography technology. Due to the infinite helical mode index of OAM mode, a large number of holographic images can be reconstructed from an OAM-multiplexing hologram. However, the traditional design of an OAM hologram is constrained by the helical mode index of the selected OAM mode, for a larger helical mode index OAM mode has a bigger sampling distance, and the crosstalk is produced for different sampling distances for different OAM modes. In this paper, we present the design of the OAM hologram based on a Bessel–Gaussian beam, which is non-diffractive and has a self-healing property during its propagation. The Fourier transform of the Bessel–Gaussian beam is the perfect vortex mode that has the fixed ring radius for different OAM modes. The results of simulation and experiment have demonstrated the feasibility of the generation of the OAM hologram with the Bessel–Gaussian beam. The quality of the reconstructed holographic image is increased, and the security is enhanced. Additionally, the anti-interference property is improved owing to its self-healing property of the Bessel-OAM holography.

Keywords: orbital angular momentum, holography, Bessel–Gaussian beam, OAM-multiplexing hologram

PACS: 42.40.–i, 42.50.Tx **DOI:** 10.1088/1674-1056/acfdff

1. Introduction

Optical holography provides a method to reconstruct both the phase and the intensity information, and becomes a promising technology to realize three-dimensional (3D) display,[1] optical encryption,[2] data storage,[3] and artificial intelligence.[4] The conventional holography uses polarization,[5] wavelength,[6,7] and time[8,9] as independent information channels, but its limited channel capacity and substantial crosstalk bring many limitations to the practical applications.[10]

Orbital angular momentum (OAM), as an independent degree of freedom, was proposed to largely improve the capacity and spectrum utilization for optical[11–13] and quantum[14,15] communication systems, since there are theoretically unbounded values of helical mode index for the OAM mode.[16] Usually, OAM mode is expressed by a helical wavefront,[17] $\exp(\mathrm{i}\ell\varphi)$, where ℓ and φ represent the helical mode index and azimuthal angle, respectively. Recently, OAM has been exploited as a new information carrier in holography to greatly improve the capacity, the security of the hologram and the data storage.[18–20] The core of the OAM holography is to preserve and select appropriate OAM modes in the reconstruction of holographic images. Therefore, the target image should be sampled by a two-dimensional (2D) Dirac comb array, where the sampling period is determined by the Fourier transform of the OAM mode.

Based on it, a partial OAM holography was proposed by dividing an OAM mode into several partial orbital angular momentums and encoded each partial mode with a different target image.[21] In 2021, an ultra-dense perfect OAM holography, in which the OAM modes were discriminated both radially and angularly was discussed.[22] The modulated chiro-optical OAM holography was proposed to further improve information security capacity, which integrated the OAM multiplexing technology with the chiro phase modulation.[23] Then, a phase gradient factor of vortex phase structure was used as an independent degree of freedom for boosting OAM holography's capacity.[24]

On the other hand, the Bessel–Gaussian beam is one of the beams carrying OAM mode (Bessel-OAM), which has the unique non-diffraction and self-healing properties.[25] Furthermore, it is shown that the perfect vortex beam with ring radius independent of topological charge can be formed by using the Fourier transform on a Bessel–Gaussian beam.[26] It seems that these advantages of the Bessel–Gaussian beam can be used in the OAM holography.

In this paper, we present the generation of an OAM holography by using Bessel–Gaussian beam. At first, we design a phase mask by combining an axicon and a helical phase function to form a Bessel–Gaussian beam. Then, we apply the op-

†Corresponding author. E-mail: zhaosm@njupt.edu.cn

© 2024 Chinese Physical Society and IOP Publishing Ltd

tical Fourier transform on the Bessel–Gaussian beam through a simple lens to form a perfect vortex beam. At the same time, the radial wave vector of the Bessel–Gaussian beam can be adjusted by controlling the axicon parameter when creating the phase mask, so as to control the ring radius of the vortex beam. After that, we demonstrate the generation of Bessel-OAM holography, including the design of Bessel-OAM preserved hologram, Bessel-OAM selective hologram and Bessel-OAM multiplexing hologram. The properties of the Bessel–Gaussian beam are added to the OAM hologram. Then, we verify the feasibility and advantages of Bessel-OAM holography by the simulations and experiments.

2. Theory

For an OAM holography, the image at first should be converted to a point image by a sampling Dirac comb array with sampling distance d, where the Dirac comb sampling array can be described as

$$\mathrm{Comb}(x,y)=\sum_{a,b}\delta[(x-x_a),(y-y_b)], \tag{1}$$

where $\delta(\cdot)$ is a unit impulse response function. (x,y) denotes the Cartesian coordinates, (x_a,y_b) represents the position of the sampling point satisfying with $x_a-x_{a-1}=d$, $y_b-y_{b-1}=d$. Consequently, the point image can be described as

$$S_k(x,y)=\mathrm{Comb}(x,y)\cdot G_k(x,y), \tag{2}$$

where $G_k(x,y)$ represents the k-th image, and $S_k(x,y)$ is the corresponding k-th point image.

Different from the spatial–frequency distributions of Laguerre–Gaussian mode in the Fourier domain, the perfect vortex beam by Fourier transformation on a Bessel–Gaussian mode has the radius independent of the incident helical mode index, that is, the helical mode index of Bessel–Gaussian mode has less effect on the sampling distance, and more OAM modes can be multiplexed in a Bessel-OAM holography. The Bessel-OAM preserved hologram $E_k(u,v)$ is then described as the Fourier transformation of the point image $S_k(x,y)$. That is,

$$E_k(u,v)=\sum_{x=1}^{M}\sum_{y=1}^{M}S_k(x,y)\exp[-\mathrm{i}2\pi(xu+yv)], \tag{3}$$

where u and v are the spatial frequencies of x and y, respectively.

Then, the Bessel-OAM selective hologram can be achieved by the interference between the point image $G_k(x,y)$ and an incident Bessel-OAM beam with the topological charge (ℓ) and the axicon parameter (a). The process can be described as

$$E_k(u,v)=\sum_{x=1}^{M}\sum_{y=1}^{M}S_k(x,y)\exp[-\mathrm{i}2\pi(xu+yv)]\times\exp\left(\mathrm{i}\frac{r}{a}\right)\exp(\mathrm{i}\ell\varphi). \tag{4}$$

With Eq. (4), the Bessel-OAM multiplexing hologram can be described as

$$E(u,v)=\sum_{k=1}^{n}\sum_{x=1}^{M}\sum_{y=1}^{M}S_k(x,y)\exp[-\mathrm{i}2\pi(xu+yv)]\times\exp\left(\mathrm{i}\frac{r}{a_k}\right)\exp(\mathrm{i}\ell_k\varphi), \tag{5}$$

where n is the number of the target images, a_k and ℓ_k are the axicon parameter and the topological charge of the Bessel-OAM beam corresponding to the k-th image, respectively. By using a computer-generated hologram (CGH) algorithm, the phase (Φ_k) can be obtained from the Bessel-OAM selective hologram. Then, the phase-only Bessel-OAM multiplexing hologram can be archived as

$$\Phi=\mathrm{angle}[\exp(\mathrm{i}\Phi_1)+\cdots+\exp(\mathrm{i}\Phi_n)], \tag{6}$$

where angle$[\cdot]$ is an operation to extract the phase of $[\cdot]$, such as Gerchberg–Saxton (GS) algorithm,[27] Φ is a real value bounded by $[0,2\pi]$.

Due to the conservation of OAM, the holographic image can only be appeared when the incident Bessel–Gaussian beam has the topological charge of $-\ell$, the axicon parameter of $-a$, and the reconstructed image has a solid-spot intensity distribution. That is

$$\begin{aligned}E(u,v)\cdot\exp\left(-\mathrm{i}\frac{r}{a_k}\right)\exp(-\mathrm{i}l_k\varphi)=&\sum_{x=1}^{M}\sum_{y=1}^{M}S_1(x,y)\exp[-\mathrm{i}2\pi(xu+yv)]\exp\left[\mathrm{i}r\left(\frac{1}{a_1}-\frac{1}{a_k}\right)\right]\exp[\mathrm{i}(l_1-l_k)\varphi]\\&\cdots\\&+\sum_{x=1}^{M}\sum_{y=1}^{M}S_k(x,y)\exp[-\mathrm{i}2\pi(xu+yv)]\exp\left[\mathrm{i}r\left(\frac{1}{a_k}-\frac{1}{a_k}\right)\right]\exp(\mathrm{i}(l_k-l_k)\varphi)\\&\cdots\\&+\sum_{x=1}^{M}\sum_{y=1}^{M}S_n(x,y)\exp[-\mathrm{i}2\pi(xu+yv)]\exp\left[\mathrm{i}r\left(\frac{1}{a_n}-\frac{1}{a_k}\right)\right]\exp[\mathrm{i}(l_n-l_k)\varphi].\end{aligned} \tag{7}$$

where the k-th holographic image with the OAM mode of ℓ_k can be turned into the Gaussian mode. By using a 2D comb function (Comb$'(x,y)$), the k-th holographic image can be filtered as, described as follows:

$$S'_k(x,y) = \mathrm{IFT}\left[E(u,v)\cdot\exp\left(-\mathrm{i}\frac{r}{a_k}\right)\exp(-\mathrm{i}l_k\varphi)\right] \times \mathrm{Comb}'(x,y), \tag{8}$$

where IFT$[\cdot]$ is the inverse Fourier transform. It is shown that different holographic images can be reconstructed when different incident Bessel-OAM beams is used.

3. Results and discussion

In this section, the simulations and experiments are carried out to verify the feasibility of the proposed generation method of the Bessel-OAM holography.

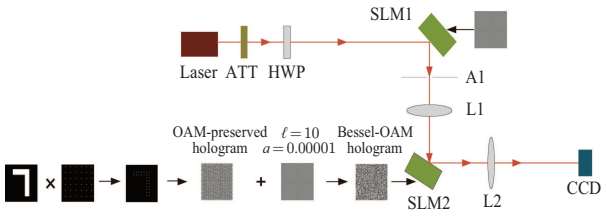


Fig. 1. The sketch of the experimental system to implement Bessel-OAM holography. ATT: attenuator, HWP: half-wave plate, L: lens, SLM: spatial light modulator, CCD: charge coupled device.

The experimental setup is shown in Fig. 1. The incident light is a linear fundamental mode Gaussian beam derived from an He–Ne laser (Thorlabs, HRS015, the power is 5 mW, the wavelength is 633 nm). An attenuator (ATT) after the laser is used to adjust the beam power, and the half-wave plate (HWP) ensures the suitable polarization direction of the incident light matches the used spatial light modulator (SLM1, Holoeye PLOTO-VIS-006-A, pixel pitch: 8 μm, pixel number: 1920×1080), on which the hologram of different Bessel–Gaussian modes is loaded. After passing through SLM1, the incident Gaussian beam is turned out a Bessel–Gaussian beam with a specific mode. By adjusting the position and size of the aperture, A1, only the first-order diffracted light can be passed through. Then, by passing A1 and a lens (L1, the focal length 150 mm), the Bessel beam with ring radius independent of topological charge can be formed, based on its Fourier transform properties. A Bessel-OAM selective hologram including the target image information and a specific Bessel mode is loaded on SLM2 (HED6010-NIR-011-C, pixel pitch: 8 μm, pixel number: 1920×1080). The holographic image can only appear when the Bessel–Gaussian mode loaded to SLM1 is opposite to that in SLM2. The reflected beam of SLM2 is Fourier transformed by lens2 (L2, the focal length 50 mm), and detected by a charge coupled Device (CCD, Thorlabs, BC106N-VIS/M). For the experimental setup, the efficiency is 14%, which is calculated by the light intensity input to CCD over the light intensity after ATT.

As shown in Fig. 1, when $\ell=10$, $a=0.0001/m$ is used in the Bessel-OAM selective hologram (in SLM2), the target image '7' can be appeared when the Bessel–Gaussian beam with $\ell=-10$, $a=-0.0001/m$ is produced by SLM1.

3.1. The feasibility

The simulation and experimental results of the holographic reconstruction for a single image are presented in Fig. 2. The hologram of the image '7' is with topological charge $\ell=5$ and axicon parameter $a=0.0001/m$. Therefore, when $a=-0.0001/m$ is fixed, different holographic reconstruction results can be achieved by different topological charges ℓ, which is shown in Fig. 2(a). Only the incident beam with $\ell=-5$ can convert the target image '7' into the Gaussian-like points, while other values of ℓ remain the target image be in ring-shape state. As shown in Fig. 2(b), when $\ell=-5$ is constant, only the incident beam with $a=-0.0001/m$ can recover the target image '7'. The simulation and experiment results show that it is feasible for the Bessel-OAM holography. Compared with the simulation results, the light intensities for different points of the experimental results (point image) are not equal. This is because the experimental results are the diffraction reconstructed optical fields, the holographic reconstructed point image is the first-order diffraction, and the light intensities of the points in the point image are affected by the zero-order diffraction spot with high-intensity, the near ones become brighter, while the far points become darker. As shown in Fig. 2(a) $\ell=-5$ experimental result, the light intensities of '7' (point image) is not the same, the light intensities of the right bottom points are bigger than those of the left upper points.

Here, we adopt cosine similarity (CS) as the metric for the image reconstruction. Cosine similarity is a measure of similarity between two vectors of an inner product space that measures the cosine of the angle between them. It is a common metric used in high-dimensional positive spaces to perform tasks such as information retrieval and data mining.[28] For two vectors $\boldsymbol{x}$ and $\boldsymbol{x}'$, CS is defined as

$$\mathrm{CS} = \frac{\boldsymbol{x}\cdot\boldsymbol{x}'}{\|\boldsymbol{x}\|\cdot\|\boldsymbol{x}'\|}, \tag{9}$$

where $\|\cdot\|$ is the modulus of the vector. Considering the pixel information in the reconstructed image may be shifted in the positions, we employ Visual Geometry Group (VGG) to extract the image features at first, then we compute the CS values on the image feature vectors.

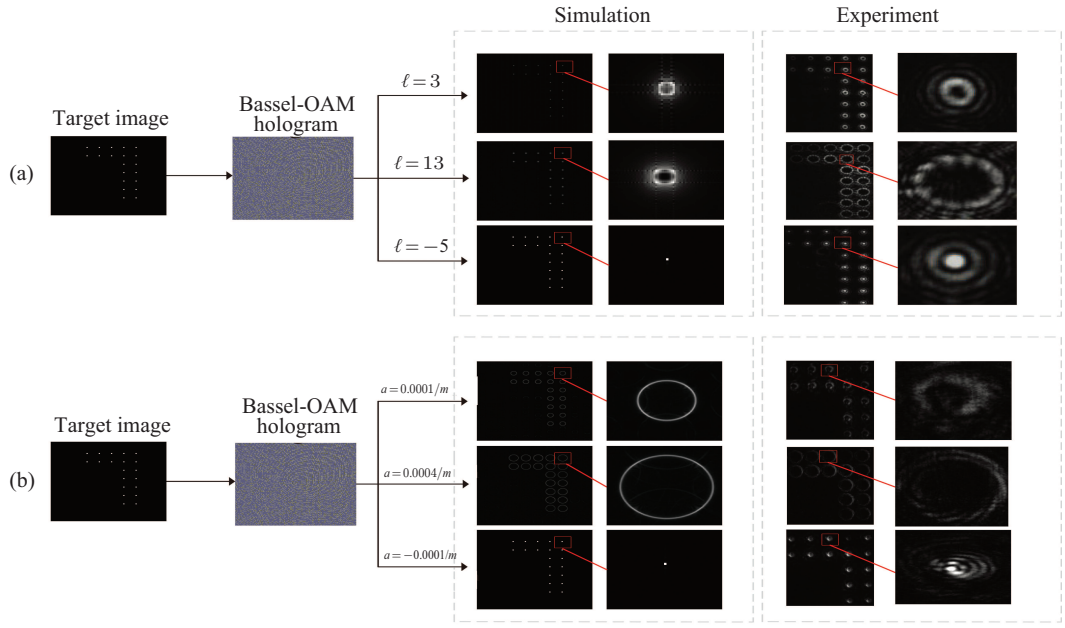


Fig. 2. The simulation and experimental results of holographic reconstruction of a single image: (a) reconstruction with different topological charges, $a=-0.0001/m$ is a constant; (b) reconstruction with different axicon parameters, $\ell=-5$ is a constant.

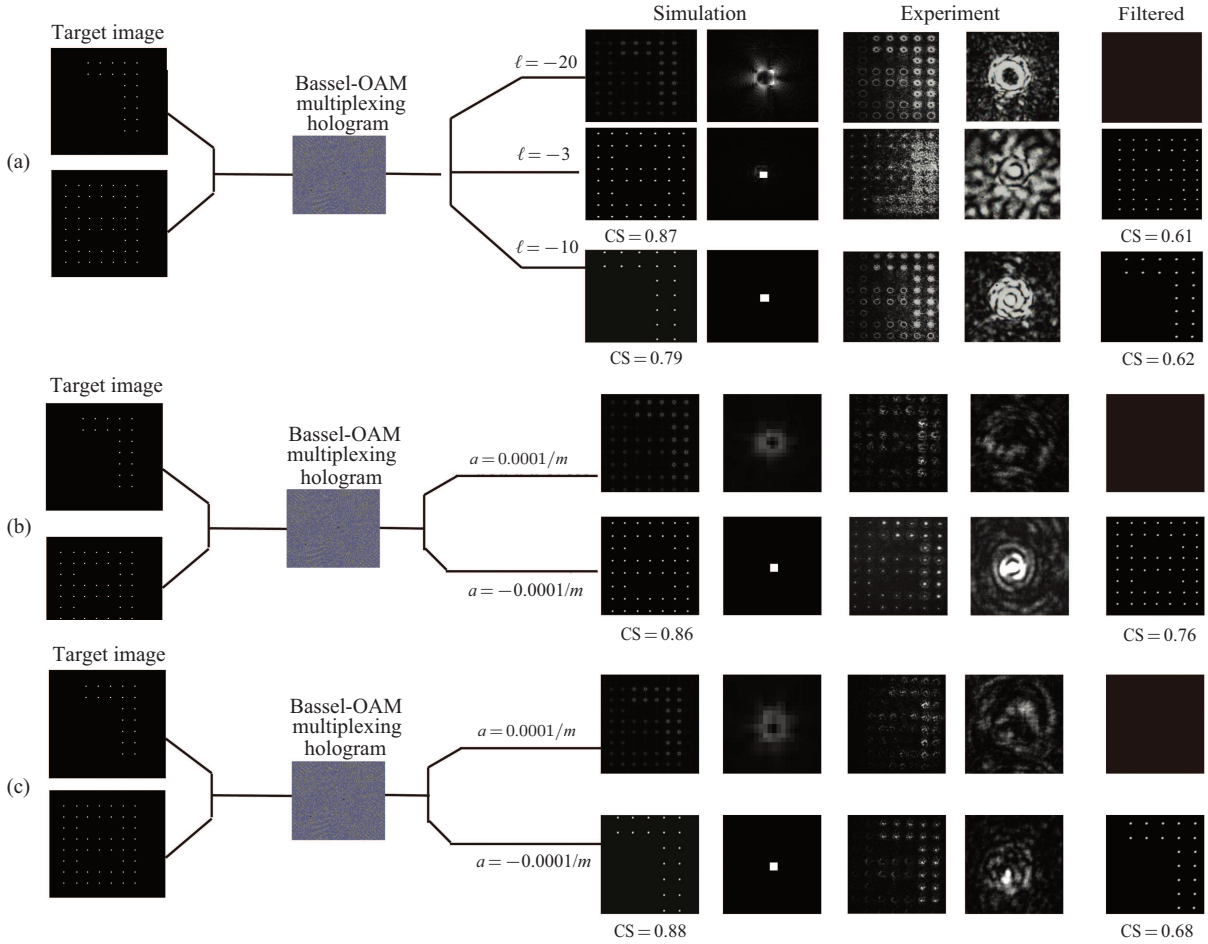


Fig. 3. The simulation and experimental results of holographic reconstruction of two overlapping images: (a) reconstruction with different topological charges, axicon parameter is $a=-0.0001/m$ (constant), (b) reconstruction with different axicon parameters, topological charge is $\ell=-3$ (constant), (c) reconstruction with different axicon parameters, topological charge is $\ell=-10$ (constant).

Based on the OAM sensitivity of the Bessel-OAM hologram, Bessel-OAM multiplexing holography can be achieved, in which different ℓ values can be assigned for different target images. Similar to the single target image holography, here, the target images '7' and '8' are assigned with different ℓ values. Figure 3 shows the Bessel-OAM-multiplexing hologra-

phy for the target images '7' and '8' with $\ell = 10$ and $\ell = 3$, respectively. It is worth noting that the positions of '7' and '8' are overlapped each other in the Bessel-OAM hologram. As shown in Fig. 3(a), if $a = -0.0001/m$ is fixed, different target images are reconstructed when the incident Bessel–Gaussian beams with different ℓ values are used. For instance, if the topological charge ℓ for the incident Bessel–Gaussian beam is -10, then the holographic image '7' is recovered. The CS values for the simulation result is 0.79, while it is 0.62 for the experimental filtered output. If the topological charge ℓ for the incident Bessel–Gaussian beam is -3, then the holographic image '8' is reconstructed. The CS values for '8' is 0.87, while it is 0.61 for the experiment. However, if the topological charge ℓ for the incident Bessel–Gaussian beam is -20, then both the holographic images '7', '8' cannot be reconstructed, they are overlapped. Similarly, as shown in Fig. 3(b) and Fig. 3(c), when ℓ is fixed, the target image only can be reconstructed when the incident Bessel–Gaussian beam is with $-a$ axicon parameter. For example, the holographic image '8' can be recovered when the incident Bessel–Gaussian beam is with $a = -0.0001/m$ for the fixed $\ell = -3$. The holographic image '7' is recovered when the incident Bessel–Gaussian beam is $a = -0.0001/m$ for the fixed $\ell = -10$. At this moment, the CS values for '8', '7' are 0.86, 0.88 for the simulation results, and 0.76 and 0.68 for the experimental results, respectively. Therefore, the high security encryption scheme can be designed by loading different images with different ℓ and different a on the Bessel-OAM-multiplexing hologram. It is worth noting that in our experimental result, the target images were located at the same positions, which was obviously the most serious crosstalk situation.

3.2. The security

Similar to the recovery of multiple overlapping images, the recovery of multiple non-overlapping images can also be achieved as shown in Fig. 4. In the same way, the target image can be filtered out by an aperture array only if the value of ℓ carried by the input light is opposite to that adopted in the target image. Otherwise, there is nothing because the target image remains in ring-shape and cannot pass through the aperture array. For instance, there are three types of images, including the linear point image, the diamond point image, and the square point image, which are encoded in the Bessel-OAM multiplexing hologram with $\ell = 3$, 10, and 15, respectively. When $\ell = -3$ Bessel–Gaussian beam is used as the incident beam, the linear point image is reconstructed with CS 0.92, the diamond point image is reconstructed with CS 0.92 when the Bessel–Gaussian beam with $\ell = -10$ is input, and the square point image is reconstructed with CS 0.94 when the Bessel–Gaussian beam with $\ell = -15$ is input. In particular, if a Gaussian beam is used as an incident beam, it can be seen that all the images appear as the rings of the same size due to the property of the perfect vortex beam. The same size output can be used to improve the security of image encryption. For instance, an image can be split up and encoded with different values of ℓ, when it is encrypted with a Bessel-OAM hologram. If a Gaussian beam is used as the incident beam, all the parts of the image appear with the same size ring. No information of the image is revealed, so that the security of the multiplexing holography is increased.

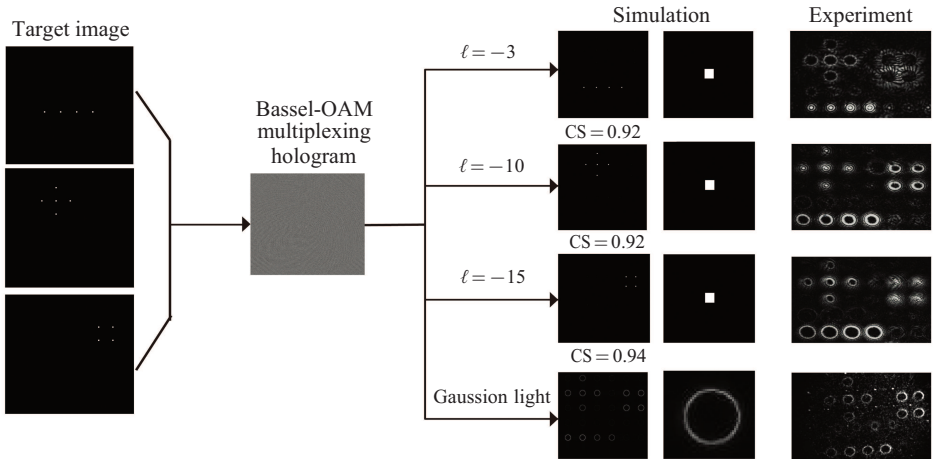


Fig. 4. The simulation and experimental results of holographic reconstruction of three non-overlapping images.

3.3. The self-healing property

The Bessel–Gaussian beam is one of the families of non-diffracting waves, which can exhibit self-healing ability during its propagation. That is to say, the Bessel–Gaussian beam has the ability to reconstruct its beam shape when it is disturbed by an obstacle. Therefore, there is a certain degree of anti-interference for the target image recovery when the Bessel-OAM holography is used. At first, we use a point-like obsta-

cle, however, the position of the obstacle is difficult to control. Then, we use a horizontal obstacle with iron wire. As shown in Fig. 5, it can be seen that the target image is composed of two complete rings when there is no obstacle. When the obstacle is placed behind the Bessel-OAM hologram, it can be seen that there are some gaps in the rings. Here, three size obstacles are used, they are 0.1 mm, 0.3 mm, and 0.5 mm, respectively. Therefore, the CS values for the images with the gap are 0.64, 0.62, and 0.55, respectively, when the propagation distance is short (50 cm). As the propagation distance increases, the gaps in the rings get smaller and smaller, and the corresponding CS values increase. When the beam from the Bessel-OAM holography passes through the obstacles and propagates to 200 cm, the gaps almost disappear for 0.1-mm size and 0.3-mm size obstacles, their CS values are 0.70 and 0.67 respectively, at the moment. However, there is a still gaps for 0.5-mm obstacle, but it is better than that propagating to 100 cm and 150 cm. It is hinted that the Bessel-OAM hologram has the self-healing property, and the property is also related with the size of the obstacle. The obstacles are very common in practical application, so that the Bessel-OAM holography has some anti-interference performance in practice.

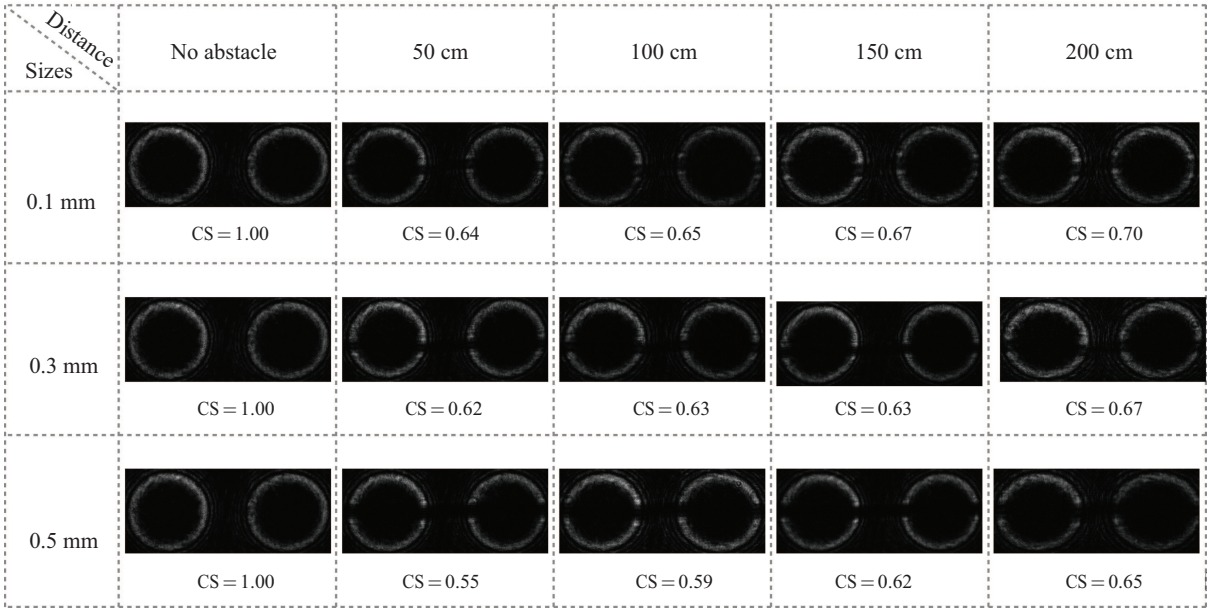


Fig. 5. Self-healing property of Bessel-OAM holography.

4. Conclusion

In this paper, we have proposed a Bessel-OAM holography scheme using the Bessel–Gaussian beam. On the one hand, the Bessel–Gaussian beam can construct the perfect vortex beam that has the fixed size ring radius by Fourier transform, so that the Bessel-OAM holography can reduce the influence of topological charge (ℓ) on the sampling interval and increase the security of OAM-multiplexing holography. On the other hand, due to the self-healing property of Bessel beam, Bessel-OAM holography has a good anti-interference property. The simulation and experimental results have shown the availability of the proposed OAM holography generation method. Both the topological charge and axicon parameters are used as the dimensionality for the OAM-multiplexing. The reconstructed holographic images' quality is increased, and the security is enhanced. Additionally, the anti-interference performance is improved owing to the self-healing property of the Bessel-OAM holography.

Acknowledgements

Project supported by the National Natural Science Foundation of China (Grant Nos. 62375140 and 62001249) and the Open Research Fund of the National Laboratory of Solid State Microstructures (Grant No. M36055).

References

[1] Blanche P A 2021 *Light: Adv. Manuf.* **2** 446
[2] Wang Y, Liu Q, Wang J and Wang Q H 2018 *Chin. Phys. B* **27** 034202
[3] Heanue J F, Bashaw M C and Hesselink L 1994 *Science* **265** 749
[4] Gu M, Fang X Y, Ren H R and Goi E 2019 *Engineering* **5** 363
[5] Wen D D, Yue F Y, Li G X, Zheng G X, Chan K L, Chen S M, Chen M, Li K F, Wong P W H, Cheah K W, Pun E Y B, Zhang S and Chen X Z 2015 *Nat. Commun.* **6** 8241
[6] Li X P, Ren H R, Chen X, Liu J, Li Q, Li C M Y, Xue G L, Jia J, Cao L C, Sahu A, Hu B, Wang Y T, Jin G F and Gu M 2015 *Nat. Commun.* **6** 6984
[7] Tahara T, Otani R, Omae K, Gotohda T, Arai Y and Takaki Y 2017 *Opt. Express* **25** 11157
[8] Demoli N, Skenderović H and Stipčević M 2015 *Opt. Lett.* **40** 4245
[9] Singh V R and Asundi A 2009 *Chin. Opt. Lett.* **7** 1117
[10] Ren H R, Fang X Y, Jang J, Bürger J, Rho J and Maier S A 2020 *Nat. Nanotechnol.* **15** 948
[11] Wang J, Yang J Y, Fazal I M, Ahmed N, Yan Y, Huang H, Ren Y X, Yue Y, Dolinar S, Tur M and Alan E W 2012 *Nat. Photon.* **6** 488

[12] Bozinovic N, Yue Y, Ren Y X, Tur M, Kristensen P, Huang H, Willner A E and Ramachandran S 2013 *Science* **340** 1545
[13] Ren H R, Li X P, Zhang Q M and Gu M 2016 *Science* **352** 805
[14] Fickler R, Lapkiewicz R, Plick W N, Krenn M, Schaeff C, Ramelow S and Zeilinger A 2012 *Science* **338** 640
[15] Wang L, Zhao S M, Gong L Y and Cheng W W 2015 *Chin. Phys. B* **24** 120307
[16] Hemsing E, Marinelli A and Rosenzweig J B 2011 *Phys. Rev. Lett.* **106** 164803
[17] Allen L, Beijersbergen M W, Spreeuw R J C and Woerdman J P 1992 *Phys. Rev. A* **45** 8185
[18] Ren H R, Briere G, Fang X Y, Ni P N, Sawant R, Héron S, Chenot S, Vézian S, Damilano B, Brändli V, Maier S A and Genevet P 2019 *Nat. Commun.* **10** 2986
[19] Fang X Y, Ren H R and Gu M 2020 *Nat. Photon.* **14** 102
[20] Zhu J L, Wang L and Zhao S M 2022 *IEEE Photon. Technol. Lett.* **35** 179
[21] Wang F L, Zhang X C, Xiong R, Ma X Y and Jiang X Q 2022 *Opt. Express* **30** 11110
[22] Zhu G X, Bai Z Y, Chen J Y, Huang C R, Wu L P, Fu C L and Wang Y P 2021 *Opt. Express* **29** 28452
[23] Li F J, Nie S P, Ma J and Yuan C J 2022 *Opt. Express* **30** 41567
[24] Li F J, Ding H, Nie S P, Ma J and Yuan C J 2023 *Opt. Lasers Eng.* **160** 107303
[25] Zhao S M, Zhang W H, Wang L, Li W, Gong L Y, Cheng W W, Chen H W and Gruska J 2019 *Sci. Rep.* **9** 2025
[26] Vaity P and Rusch L 2015 *Opt. Lett.* **40** 597
[27] Wu Y, Wang J, Chen C, Liu C J, Jin F M and Chen N 2021 *Opt. Express* **29** 1412
[28] Xia P, Zhang L and Li F 2015 *Info. Sci.* **307** 39